Applied Catalysis B: Environmental 86 (2009) 36–44

Contents lists available at ScienceDirect

Applied Catalysis B: Environmental

journal homepage: www.elsevier.com/locate/apcatb

# Promoting effect of MgO addition to $Pt/Ni/CeO_2/Al_2O_3$ in the steam gasification of biomass

Kazuya Nakamura [a], Tomohisa Miyazawa [a], Takuya Sakurai [a], Toshihiro Miyao [b], Shuichi Naito [b], Noorjahan Begum [a], Kimio Kunimori [a], Keiichi Tomishige [a,*]

[a] Institute of Material Sciences, University of Tsukuba, 1-1-1 Tennodai, Tsukuba, Ibaraki 305-8573, Japan
[b] Department of Applied Chemistry, Faculty of Engineering, Kanagawa University, 3-27-1 Rokkakubashi, Kanazawa-ku, Yokohama, Kanagawa 221-8686, Japan

ARTICLE INFO

*Article history:*
Received 14 March 2008
Received in revised form 7 July 2008
Accepted 17 July 2008
Available online 25 July 2008

*Keywords:*
Steam gasification
Biomass
Steam reforming
Tar
Regeneration
Re-dispersion
Ni
MgO
Solid solution
Synthesis gas

ABSTRACT

$Pt/Ni/CeO_2/Al_2O_3$ catalyst showed the high performance in the steam gasification of cedar wood at the initial stage, however, the catalyst was deactivated within 2 h. According to the catalyst characterization by means of XRD and Ni *K*-edge EXAFS, it is found that aggregation of Ni metal particles causes the deactivation. In contrast, the $Pt/Ni/CeO_2/MgO/Al_2O_3$ showed the high catalytic activity and stability. The addition of MgO to $Pt/Ni/CeO_2/Al_2O_3$ decreased the reduction degree of Ni, but increased the dispersion of the Ni metal particles. As a result, the activity of $Pt/Ni/CeO_2/MgO/Al_2O_3$ was comparable to that of $Pt/Ni/CeO_2/Al_2O_3$. The $Pt/Ni/CeO_2/MgO/Al_2O_3$ had high resistance to the aggregation, which can be related to high stability. Another important point is that the aggregated Ni particles on the $Pt/Ni/CeO_2/MgO/Al_2O_3$ became re-dispersed by the catalyst regeneration (oxidation and reduction). The re-dispersion can proceed via the formation of the NiO–MgO solid solution by oxidation and the reduction of the NiO–MgO from the results of XRD and Ni *K*-edge EXAFS.



## 1. Introduction

Biomass can be an abundantly available and renewable energy resource. Conversion of biomass to synthesis gas and hydrogen contributes to the environmental protection by the decrease of $CO_2$ emission [1,2]. This is because the synthesis gas can be converted to clean liquid fuels, such as methanol, and Fischer-Tropsch oil, and hydrogen is a promising energy carrier in the future. Catalytic gasification of biomass with air and oxygen is an effective method for the production of synthesis gas with smaller tar content [3–16]. Since air has been used as a gasifying agent in a practical case, the synthesis gas by the biomass gasification with air was diluted with nitrogen, which can be a negative factor in the utilization of the synthesis gas. In contrast, in the case of steam gasification and steam reforming, the concentration of the synthesis gas in the product gas can be much higher. Therefore, the catalysts for the steam gasification and tar reforming have been developed [17–29].

It has also been reported that $Rh/CeO_2/SiO_2$ was effective in steam gasification of biomass [3,19,20]. However, the catalyst has problems in terms of the high cost and limited availability originated from the usage of Rh. Another promising candidate of active components is Ni. As mentioned above, since it has been known that the coke deposition is a serious problem of Ni catalysts in the syngas production process [30–33], it is necessary to design the catalyst with high resistance to coke deposition. Recently, we have investigated coke deposition behavior over various oxides supported Ni catalysts in the steam gasification of cedar wood [21]. It is characteristic that $Ni/CeO_2$ was effective to the suppression of coke deposition [21]. The performance on $Ni/CeO_2/Al_2O_3$ catalysts prepared by co-impregnation and sequential impregnation methods was compared, in the steam gasification of cedar wood [22,23]. In particular, the $Ni/CeO_2/Al_2O_3$ catalyst prepared by the co-impregnation method was much more effective than that by the sequential impregnation method. Characterization results indicated that the interaction between Ni metal particles and $CeO_2$ is stronger on the catalyst prepared by the co-impregnation method, on which the composite of Ni metal and $CeO_2$ is formed. The interaction between Ni and $CeO_2$ enhances the catalytic reforming activity with high resistance to coke formation, and it can

* Corresponding author. Tel.: +81 298 53 5030; fax: +81 298 53 5030.
*E-mail address:* tomi@tulip.sannet.ne.jp (K. Tomishige).

0926-3373/$ – see front matter © 2008 Elsevier B.V. All rights reserved.
doi:10.1016/j.apcatb.2008.07.016

contribute to the decrease of the tar and coke yields. Moreover, the additive effect of a small amount of noble metals such as Pt, Rh, Ru and Pd over the $Ni/CeO_2/Al_2O_3$ catalysts prepared by the co-impregnation method was investigated [24,25]. The addition of Pt was much more effective than Rh, Ru and Pd. In particular, the $Pt/Ni/CeO_2/Al_2O_3$ catalyst without $H_2$ reduction treatment exhibited similar catalytic performance to that after the $H_2$ reduction pretreatment. Characterization results indicated that the Pt species can interact with Ni species much more strongly than other noble metals, and the Pt–Ni alloy formation was detected in the EXAFS analysis.

In this article, we investigated the life of the $Pt/Ni/CeO_2/Al_2O_3$ catalyst in the steam gasification of cedar wood, and the catalyst deactivation was observed. Here, the additive effect of MgO to the $Pt/Ni/CeO_2/Al_2O_3$ was evaluated, and it is found that the addition of MgO enhanced the catalyst stability by the promotion of the Ni dispersion and the re-dispersion of the aggregated Ni metal particles during the regeneration procedure.

## 2. Experimental

### 2.1. Catalyst preparation

The $Ni/CeO_2/Al_2O_3$ catalyst was prepared by a co-impregnation method using the mixed aqueous solution of $Ni(NO_3)_2{\cdot}6H_2O$ and $Ce(NH_4)_2(NO_3)_6$. Before the impregnation, $Al_2O_3$ (JRC-ALO-1, Catalysis Society of Japan, 143 $m^2\,g^{-1}$, grain size 2–3 mm) was calcined in air at 1473 K to change from $\gamma$-$Al_2O_3$ to $\alpha$-$Al_2O_3$. After that, it was crushed and sieved to particle sizes between 0.6 and 2.0 mm. The co-impregnation was carried out by the incipient wetness method. After the impregnation, the sample was dried at 383 K for 12 h followed by the calcination at 773 K for 3 h under air atmosphere. On the other hand, the $Ni/CeO_2/MgO/Al_2O_3$ and $Ni/MgO/Al_2O_3$ were also prepared by the incipient wetness method using the aqueous solution of $Ni(NO_3)_2{\cdot}6H_2O$, $Ce(NH_4)_2(NO_3)_6$, and $Mg(NO_3)_2{\cdot}6H_2O$ and the $Al_2O_3$. The procedures for the drying and the calcination were just the same as those used for the $Ni/CeO_2/Al_2O_3$. The $Ni/CeO_2/Al_2O_3$, $Ni/CeO_2/MgO/Al_2O_3$ and $Ni/MgO/Al_2O_3$ are denoted as Ni/CA, Ni/CMA and Ni/MA, respectively. Pt was loaded on the $Ni/CeO_2/Al_2O_3$, $Ni/CeO_2/MgO/Al_2O_3$ and $Ni/MgO/Al_2O_3$, by the incipient wetness method using the aqueous solution of $Pt(NO_2)_2(NH_3)_2$. After this procedure, the samples were dried at 383 K for 12 h, followed by the calcination at 773 K for 3 h under air atmosphere again. The catalysts are denoted as Pt/Ni/CA, Pt/Ni/CMA and Pt/Ni/MA. All these catalysts were sieved again to granules with the size of 0.6–2.0 mm. The loading amount of Ni, $CeO_2$, MgO, and Pt was 12 wt%, 15 wt%, 2 wt%, and 0.1 wt%, respectively. The loading amount of Pt and Ni was based on our previous report [25].

### 2.2. Biomass

Cedar wood was ground with a ball mill to about 0.1–0.3 mm size. The moisture content of the cedar wood was 9.2%. The dry-based composition by weight was C 51.1%, H 5.9%, O 42.5%, N 0.1%, and ash 0.3%. The elemental analysis was carried out by the Japan Institute of Energy.

### 2.3. Activity test in the steam gasification of cedar wood

Activity tests were carried out in a laboratory-scale continuous feeding dual-bed reactor. The reactor contained the primary bed for pyrolysis of the cedar and accumulation of solid products in the pyrolysis reaction such as char and ash. The pyrolysis products in the gas phase at the reaction temperature can include tar, and they were introduced to the secondary catalyst bed. Here, the steam gasification of biomass means the pyrolysis and subsequent catalytic steam reforming of the tar derived from the pyrolysis of the biomass. The structure of the reactor and the details of the procedure for catalytic performance evaluation in the steam gasification have been already described in our previous report [23]. Feeding rate of gases, steam and biomass is described in each result. In the reaction, carbon-containing solid byproducts were observed. Char originated from the pyrolysis of the cedar was accumulated in the primary bed. On the other hand, the solid carbon deposited on the catalysts is called coke. The method for determining char and coke amount was the same as that in our previous report [23]. The reaction temperature was controlled by the thermocouple positioned outside the reactor near the catalyst bed. The tests were carried out under atmospheric pressure by using 1 g of catalyst. We evaluated the catalytic performance over the catalysts with and without reduction pretreatment at 773 K for 0.5 h using 30 ml/min $H_2$. The effluent gas was collected by a syringe and analyzed by gas chromatograph (GC) in the similar way to that reported [23]. The carbon-based conversion to gas (C-conversion) and the yield of coke, char and tar were estimated on the basis of our previous report [23]. In addition, we used the formation rate of $CO + H_2 + 4CH_4$ for the comparison, where 4 times of $CH_4$ is based on the reaction formula of $CH_4 + H_2O \rightarrow CO + 3H_2$. In addition, the activity test for longer reaction time was also carried out for the evaluation of the catalyst stability. In this activity test, the amount of the deposited coke was estimated by using thermogravimetric analysis (TGA, Shimadzu DTA-60). The samples used were about 40 mg catalysts after the life test. Each TGA profile was measured under flowing air (20 ml/min) at the heating rate of 10 K/min. An exothermic weight loss was observed at the temperature range between 750 and 950 K. This can be assigned to the combustion of the deposited coke. It is possible to estimate the amount of coke deposition on the basis of this weight loss. The catalysts after the reaction and regeneration were used for the characterization. Regeneration procedure includes the oxidation treatment at 873 K using 30 ml/min $O_2$ and 60 ml/min $N_2$ for 0.25 h in order to remove the deposited coke and the reduction treatment at 773 K using 30 ml/min $H_2$ for 0.5 h.

### 2.4. Catalyst characterization

Surface area of catalysts was measured by BET method. Chemisorption experiments were carried out in a high-vacuum system by volumetric methods. Before $H_2$ adsorption measurement, the catalysts were treated in $H_2$ at 773 K for 0.5 h, and evacuated at 723 K. $H_2$ adsorption was performed at room temperature. Gas pressure at adsorption equilibrium was about 1.1 kPa. The sample weight was about 0.2 g. The dead volume of the apparatus was about 60 $cm^3$.

Temperature-programmed reduction (TPR) with $H_2$ was performed in the fixed-bed flow reactor. The TPR profile of each sample was recorded from room temperature to 1273 K under a flow of 5.0% $H_2$/Ar, and the flow rate was 30 ml/min. The catalyst weight was 0.2 g. The heating rate was 10 K/min and the temperature was maintained at 1273 K for 30 min after it reached 1273 K. The consumption of $H_2$ was monitored continuously with TCD gas chromatograph equipped with frozen acetone trap in order to remove $H_2O$ from the effluent gas.

Transmission electron microscope (TEM) photographs were taken by means of JEM-2010 (JEOL) equipment operated at 200 kV. The sample powders after the reduction, the reaction and the regeneration were dispersed in 2-propanol by super-

sonic wave and put on Cu grids for TEM observation under atmosphere.

Powder X-ray diffraction (XRD) patterns of samples after the reduction ($H_2$ flow, 773 K, 0.5 h), the reaction and the regeneration were collected on a Philips X'pert diffraction-meter using Cu Kα (λ = 0.154 nm) generated at 40 kV and 20 mA.

Ni *K*-edge extended X-ray absorption fine structure (EXAFS) was measured at the BL-9C station of the Photon Factory at the High Energy Accelerator Research Organization in Tsukuba, Japan (Proposal No. 2004G280). The storage ring was operated at 2.5 GeV with ring current of 300–450 mA. A Si(1 1 1) single crystal was used to obtain monochromatic X-ray beam. The monochromator was detuned to 60% of the maximum intensity to avoid higher harmonics in the X-ray beam. Two ion chambers filled with $N_2$ and 15% Ar diluted with $N_2$ were used as detectors of $I_0$ and $I$, respectively. The samples for the EXAFS measurement were prepared by pressing the mixture of the catalyst with the same amount of α-$Al_2O_3$ powder to the disk with 20–25 mg. The thickness of the samples was chosen to be 0.2–0.4 mm (7 mm Ø) to give edge jump of 0.9–1.6. After the reduction and the regeneration, the samples were transferred to the measurement cell without exposing the sample disk to air using a glove box filled with nitrogen. On the other hand, the sample after the reaction was pressed into a disk under air atmosphere. EXAFS data were collected in a transmission mode at room temperature. For EXAFS analysis, the oscillation was first extracted from the EXAFS data by a spline smoothing method [34]. The oscillation was normalized by the edge height around 50 eV. The Fourier transformation of the $k^3$-weighted EXAFS oscillation from *k* space to *r* space was performed over the range of 30–160 $nm^{-1}$ to obtain a radial distribution function. The inversely Fourier filtered data were analyzed by a usual curve fitting method [35,36]. For the curve fitting analysis, the empirical phase shift and amplitude functions for the Ni–Ni bond were extracted from the data for Ni foil. The empirical phase shift and amplitude functions for the Ni–O and Ni–O–Ni bonds were extracted from the date for NiO. Theoretical functions for the Ni–O–Mg bond were calculated using the FEFF8.2 program [37]. The analysis of EXAFS data was performed using the "REX2000" program (RIGAKU Co. Version: 2.3.3).

## 3. Results and discussion

Fig. 1 shows catalytic performance in steam gasification of biomass over Ni/CA, Ni/CMA and Ni/MA catalysts. The performance was evaluated for 15 min in the activity test. The formation rate of the gaseous products was almost stable during 15 min, although the coke deposition was observed as shown in Fig. 1. The amount of coke on Ni/CA at 823 K was estimated to be 4 wt% as the ratio of carbon weight to the catalyst weight. The amount of coke was so small that the deactivation was not observed in the present case. Therefore, the results are based on the average formation rates of these products for 15 min. On all these three catalysts, the yield of the gases increased and the yield of coke and char decreased with increasing reaction temperature. The difference in the catalytic performance among the catalysts was larger at lower reaction temperature. Judging from the tar yield, the order of the catalytic activity in the steam reforming of tar is as follows: Ni/CA > Ni/CMA > Ni/MA. This result indicates that the $CeO_2$ addition is essential for high performance [22,23]. Although the details are not shown, the 4 wt% MgO addition to Ni/CA decreased the catalytic activity, and the optimum of the MgO loading amount was determined to be 2 wt%.

Fig. 2 shows catalytic performance over Pt/Ni/CA, Pt/Ni/CMA and Pt/Ni/MA. The comparison between Figs. 1 and 2 gives the additive effect of Pt. It should be noted that Pt/$CeO_2$/$Al_2O_3$ has low

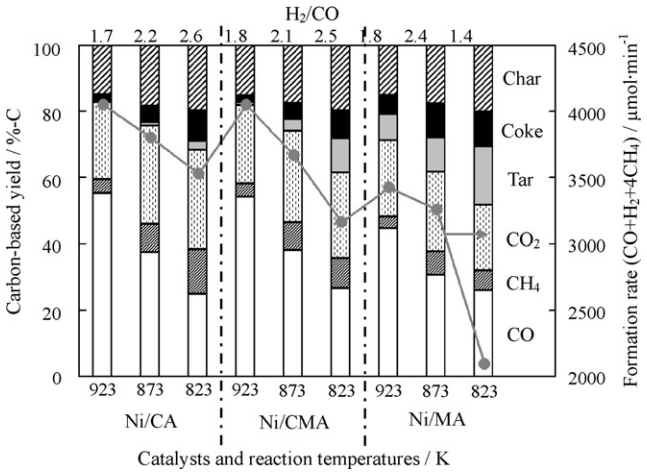


**Fig. 1.** Catalytic performance in steam gasification of cedar wood over the catalysts after $H_2$ reduction. Conditions: biomass; 60 mg/min ($H_2O$ 9.2%, C 2191 μmol/min; H 3543 μmol/min; O 1475 μmol/min), $N_2$ flow rate; 60 ml/min, (added $H_2O$)/C = 0.5 (steam flow rate 1110 μmol/min), reaction time; 15 min, $H_2$ reduction 773 K, 30 min.

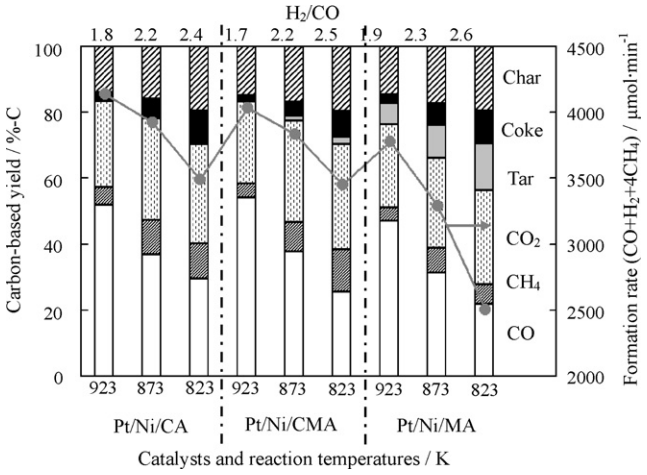


**Fig. 2.** Catalytic performance in steam gasification of cedar wood over the catalysts after $H_2$ reduction. Conditions: biomass; 60 mg/min ($H_2O$ 9.2%, C 2191 μmol/min; H 3543 μmol/min; O 1475 μmol/min), $N_2$ flow rate; 60 ml/min, (added $H_2O$)/C = 0.5 (steam flow rate 1110 μmol/min), reaction time; 15 min, $H_2$ reduction 773 K, 30 min.

activity in the steam gasification because of very small loading amount as reported previously [25]. Therefore, it is concluded that the active species for steam reforming is Ni. The contribution of Pt itself to the activity of the steam reforming of tar is rather small, and the role of Pt is to enhance the activity of Ni as discussed below [24,25]. The order of the activity is as follows: Pt/Ni/CA ≈ Pt/Ni/CMA > Pt/Ni/MA. The addition of Pt to Ni/CMA enhanced the catalytic activity remarkably, and as a result, the performance of Pt/Ni/CMA became comparable to that of Pt/Ni/CA.

Fig. 3 demonstrates the formation rate of the products as a function of time on stream over Pt/Ni/CA and Pt/Ni/CMA in steam gasification without $H_2$ reduction pretreatment. As reported previously, the addition of Pt to Ni/CA made the $H_2$ reduction pretreatment unnecessary [24,25], and in fact, the formation rate was stable from the initial stage (Fig. 3a). On the other hand, the formation rate over Pt/Ni/CMA increased with time on stream, and it reached the similar formation rate to that over Pt/Ni/CMA with the $H_2$ reduction pretreatment after 12 min (Fig. 3b). The results indicate that the tar derived from the pyrolysis of cedar wood can

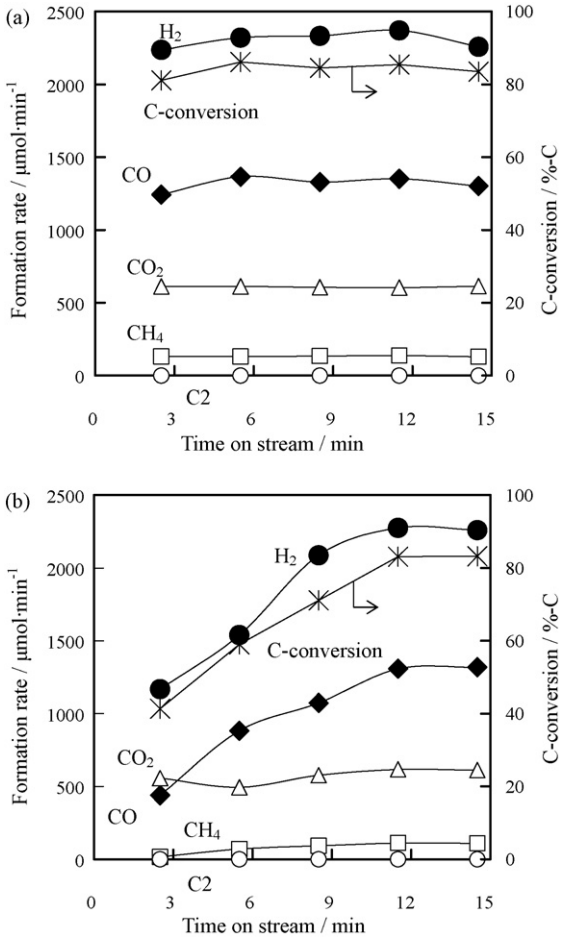


**Fig. 3.** Catalytic performance in steam gasification of cedar wood at 923 K as a function of time on stream over the catalysts without $H_2$ reduction. (a) Pt/Ni/CA and (b) Pt/Ni/CMA. Conditions: biomass; 60 mg/min ($H_2O$ 9.2%, C 2191 μmol/min; H 3543 μmol/min; O 1475 μmol/min), $N_2$ flow rate; 60 ml/min, (added $H_2O$)/C = 0.5 (steam flow rate 1110 μmol/min).

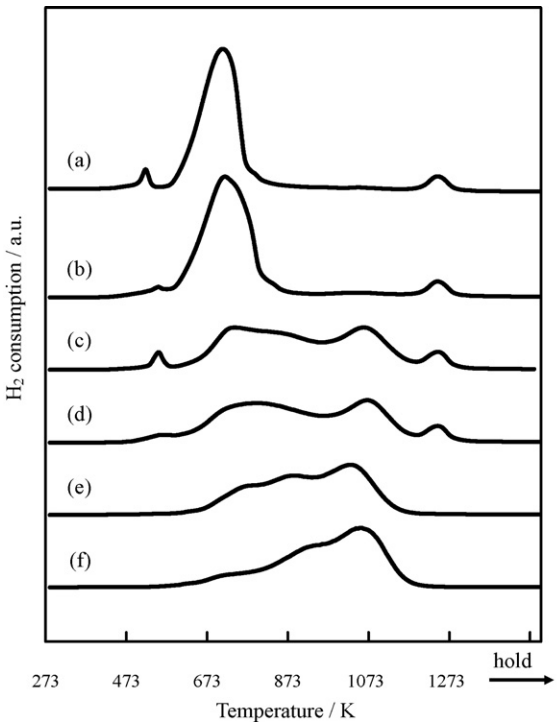


**Fig. 4.** TPR profiles of the catalysts. (a) Pt/Ni/CA; (b) Ni/CA; (c) Pt/Ni/CMA; (d) Ni/CMA; (e) Pt/Ni/MA; (f) Ni/MA. TPR condition: heating rate 10 K/min, room temperature to 1273 K, and the temperature was maintained at 1273 K for 30 min. 5% $H_2$/Ar flow rate 30 ml/min. Sample weight: 200 mg.

reduce the catalysts although the reduction of Pt/Ni/CMA was not so rapid as that of Pt/Ni/CA. This behavior indicates that the catalysts can be activated automatically by the reactants, which is regarded as the ability of the self-activation [38–40].

Fig. 4 shows the TPR profiles of the calcined catalysts, and the peak area in the TPR profiles can give the amount of $H_2$ consumption. Since the temperature for the $H_2$ reduction pretreatment is 773 K, the amount of $H_2$ consumption below 773 K and the Ni-based reduction degree estimated from the amount of $H_2$ consumption is also listed in Table 1. On Ni/CA and Pt/Ni/CA, the reduction proceeds mainly below 773 K. The peak was shifted to 10 K lower temperature by the addition of Pt. The tendency is similar to that reported previously [24,25]. The profiles of Ni/CMA and Pt/Ni/CMA were greatly different from those of Ni/CA and Pt/Ni/CA, which and this can be explained by the effect of the presence of MgO. On Ni/CMA and Pt/Ni/CMA, the temperature range of the $H_2$ consumption was much broader. The TPR profiles of Ni/MA and Pt/Ni/MA were also obtained, and the main peak was located at about 1073 K. As reported previously, the NiO on α-$Al_2O_3$ can be reduced below 873 K [22–24,41]. Based on the result, it is interpreted that the presence of MgO decreases the reducibility of Ni species and it can be caused by the strong interaction between NiO and MgO obtained by the formation of NiO–MgO solid solution [42]. The molar ratio of MgO to NiO is only 1/4, however the effect of MgO is rather strong. The Ni-based reduction degree on Ni/CA and Pt/Ni/CA below 773 K decreased significantly to about 1/3 by the addition of MgO. This tendency was more remarkable on Ni/MA and Pt/Ni/MA. In addition, the amount of $H_2$ adsorption on fresh catalysts is also listed in Table 1. The amount of $H_2$ adsorption

**Table 1**
Properties of the catalysts after $H_2$ pretreatment at 773 K

| Catalysts | BET surface area ($m^2\ g^{-1}$ cat) | $H_2$ consumption[a] ($\times10^{-3}$ mol $g^{-1}$ cat) | Ni-based reduction degree[b] (%) | $H_2$ adsorption[c] ($\times10^{-5}$ mol $g^{-1}$ cat) | Dispersion[d] (%) | Particle size of Ni metal[e] (nm) |
|---|---|---|---|---|---|---|
| Ni/CA | 17.4 | 1.40 | 89 | 4.1 | 5.9 | 16.6 |
| Pt/Ni/CA | 18.8 | 1.51 | 96 | 4.2 | 5.6 | 17.5 |
| Ni/CMA | 17.6 | 0.46 | 29 | 4.1 | 17.8 | 5.4 |
| Pt/Ni/CMA | 19.2 | 0.47 | 30 | 3.9 | 16.6 | 5.9 |
| Ni/MA | 9.0 | 0.16 | 10 | 2.6 | 32.5 | 3.0 |
| Pt/Ni/MA | 9.1 | 0.24 | 15 | 2.4 | 20.0 | 4.9 |

[a] $H_2$ consumption below 773 K in TPR profiles shown in Fig. 3.
[b] Based on the assumption that $Ni^{2+} + H_2 \rightarrow Ni^0 + 2H^+$, and the reduction of Pt and $CeO_2$ was neglected.
[c] $H_2$ adsorption is total adsorption at room temperature, and H/Ni = 1 is assumed.
[d] 2 × ($H_2$ adsorption)/($H_2$ consumption) × 100.
[e] Particle size of Ni metal is calculated by the relation: (particle size/nm) = 9.71/(dispersion/%) × 10.

on Ni/CMA and Pt/Ni/CMA was almost the same as that on Ni/CA and Pt/Ni/CA, although the reduction degree was much lower. This behavior indicates that the MgO addition promotes the dispersion of Ni metal particles, although it decreases the reduction degree of Ni species. The negative effect can be compensated by the promoting effect. The amount of $H_2$ adsorption on Ni/MA and Pt/Ni/MA was much smaller than that on other catalysts, and this can be connected to lower catalytic performance in the steam gasification (Figs. 1 and 2). Furthermore, the TPR profiles of Pt/Ni/CA and Pt/Ni/CMA are also related to the behavior in steam gasification on the catalysts without $H_2$ reduction. The reducibility of Pt/Ni/CA is much higher than that of Pt/Ni/CMA. The slower activation process by the tar over Pt/Ni/CMA is explained by the lower reducibility. The dispersion of Ni metal particles can be expected if it is assumed that $H_2$ is consumed by the reduction of Ni and the stoichiometric ratio of hydrogen atom to surface Ni atom is equal to 1. The assumptions are valid because the molar ratio of Pt and Ce to Ni is 1/400 and 1/2, respectively. Based on these assumptions, the dispersion is calculated and listed in Table 1. The dispersion of the Pt/Ni/CMA is higher than that of Pt/Ni/CA, and the Ni metal particle size is smaller as listed in Table 1. Another important point is that that small peak at almost 573 K on Pt/Ni/CA and Pt/Ni/CMA was observed. The $H_2$ consumption due to this peak was 20 times larger than that for the reduction of the Pt species ($Pt^{2+} \rightarrow Pt^0$). This suggests that the $H_2$ is consumed by the reduction of Ni and Ce species. According to our previous report, this $H_2$ consumption is assigned to the reduction of Ni because the peak was not observed on $Pt/CeO_2/Al_2O_3$, and the Pt–Ni alloy formation was detected by the Pt $L_3$-edge EXAFS analysis [24,25]. This property is reflected by high reducibility of Pt and its high ability to form spilt-over hydrogen [43,44]. Therefore, it is expected that hydrogen atom can be supplied from surface Pt atoms to surface Ni atoms easily over Pt–Ni alloy particles. It can promote hydrogenation of carbonaceous species derived from tar on surface Ni atoms, which can contribute to the suppression of the Ni deactivation.

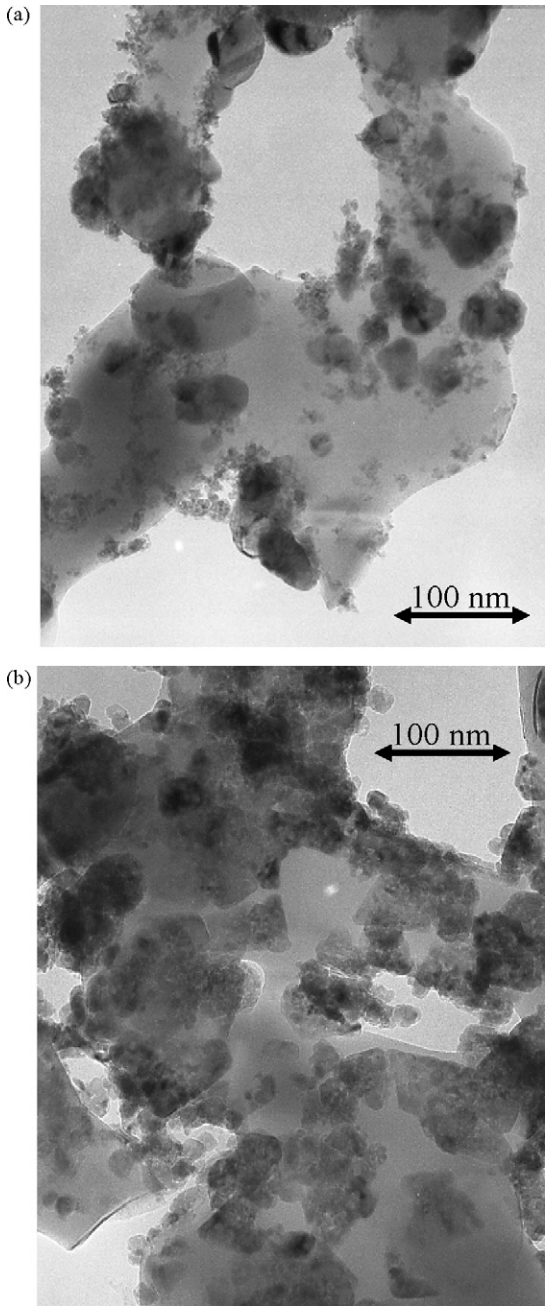


**Fig. 5.** TEM images of the catalysts after $H_2$ pretreatment at 773 K. (a) Pt/Ni/CA and (b) Pt/Ni/CMA.

Fig. 5 shows the TEM images of Pt/Ni/CA and Pt/Ni/CMA after $H_2$ reduction pretreatment at 773 K. Large particles (>20 nm) were often observed on Pt/Ni/CA, in contrast, smaller particles were mainly observed on the Pt/Ni/CMA. These support the dispersion estimated from the TPR and $H_2$ adsorption (Table 1).

Fig. 6 shows the formation rate of gaseous products and C-conversion as a function of time on stream in steam gasification of biomass over the Pt/Ni/CA and Pt/Ni/CMA catalysts at 923 K when the molar ratio of added steam to carbon in the biomass is equal to 0.5. The formation rate and C-conversion on Pt/Ni/CA decreased

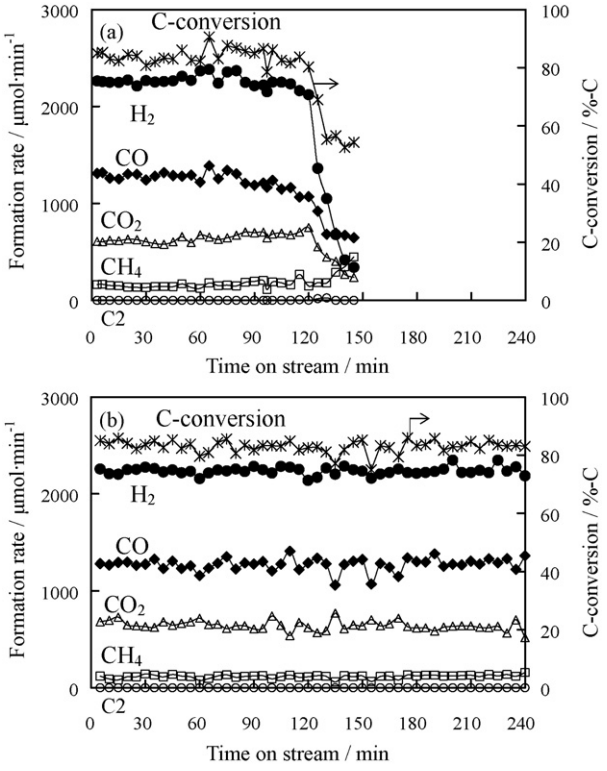


**Fig. 6.** Catalytic performance in steam gasification of cedar wood as a function of time on stream over the catalysts at 923 K. (a) Pt/Ni/CA and (b) Pt/Ni/CMA. Conditions: biomass; 60 mg/min ($H_2O$ 9.2%, C 2191 μmol/min; H 3543 μmol/min; O 1475 μmol/min), $N_2$ flow rate; 60 ml/min, (added $H_2O$)/C = 0.5 (steam flow rate 1110 μmol/min), $H_2$ reduction at 773 K, 30 min.

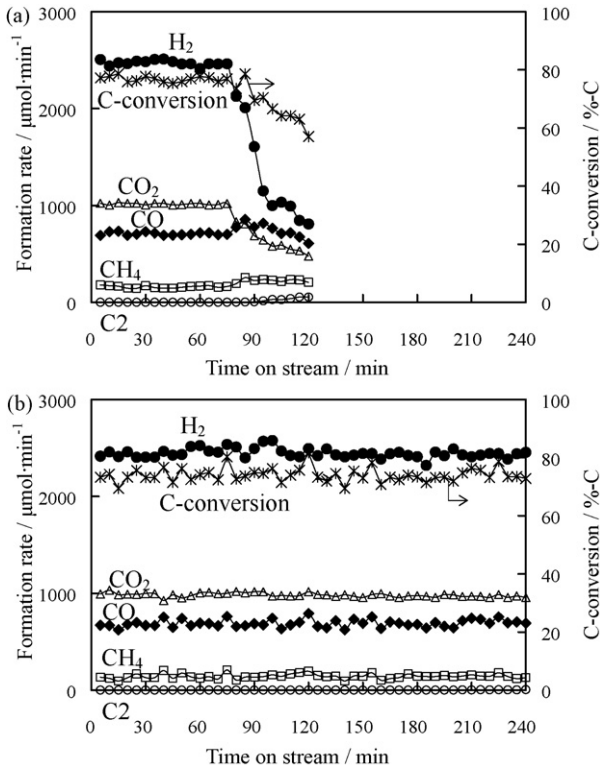


**Fig. 7.** Catalytic performance in steam gasification of cedar wood as a function of time on stream over the catalysts at 873 K. (a) Pt/Ni/CA and (b) Pt/Ni/CMA. Conditions: biomass; 60 mg/min ($H_2O$ 9.2%, C 2191 μmol/min; H 3543 μmol/min; O 1475 μmol/min), $N_2$ flow rate; 60 ml/min, (added $H_2O$)/C = 1 (steam flow rate 2220 μmol/min), $H_2$ reduction at 773 K, 30 min.

drastically at about 120 min, and this behavior corresponds to catalyst deactivation. On the other hand, the Pt/Ni/CMA maintained high activity even after 240 min. As shown in Fig. 2, the activity of Pt/Ni/CMA was almost the same as that of Pt/Ni/CA. Considering the catalytic activity, the difference in the reaction time dependence between Pt/Ni/CMA and Pt/Ni/CA can be reflected by the catalyst stability.

Fig. 7 shows the formation rate of gaseous products and C-conversion over Pt/Ni/CA and Pt/Ni/CMA at 873 K when the molar ratio of added steam to the carbon in the biomass is equal to 1. Under these reaction conditions, the Pt/Ni/CA catalyst was deactivated after 80 min. The Pt/Ni/CMA showed more stable activity even after 240 min. Under both reaction conditions, the Pt/Ni/CMA exhibited much higher stability than Pt/Ni/CA. It is found that the addition of MgO is effective to the enhancement of catalysts stability rather than the activity. One possible reason of the deactivation can be coke deposition. The amount of coke after the reaction shown in Fig. 6 on Pt/Ni/CA and Pt/Ni/CMA was measured to be 4 wt% and 3 wt%, respectively, by the thermogravimetric method. These coke amounts were too small to deactivate the catalysts.

Fig. 8 shows the XRD patterns of Pt/Ni/CA and Pt/Ni/CMA after the $H_2$ reduction, reaction and regeneration. The results were normalized by the peak due to α-$Al_2O_3$ at $2\theta = 35.1^\circ$. The peaks assigned to Ni and $CeO_2$ were observed, however no peaks due to MgO were observed at all. The average particle size of the Ni metal can be estimated on the basis of line broadening analysis using Sherrer equation [45]. The average Ni particle size on Pt/Ni/CA after the reduction was determined to be 18.7 nm, and this agrees well with that obtained from the adsorption and the TPR as listed in Table 1. The average particle size of Pt/Ni/CA after the reaction and

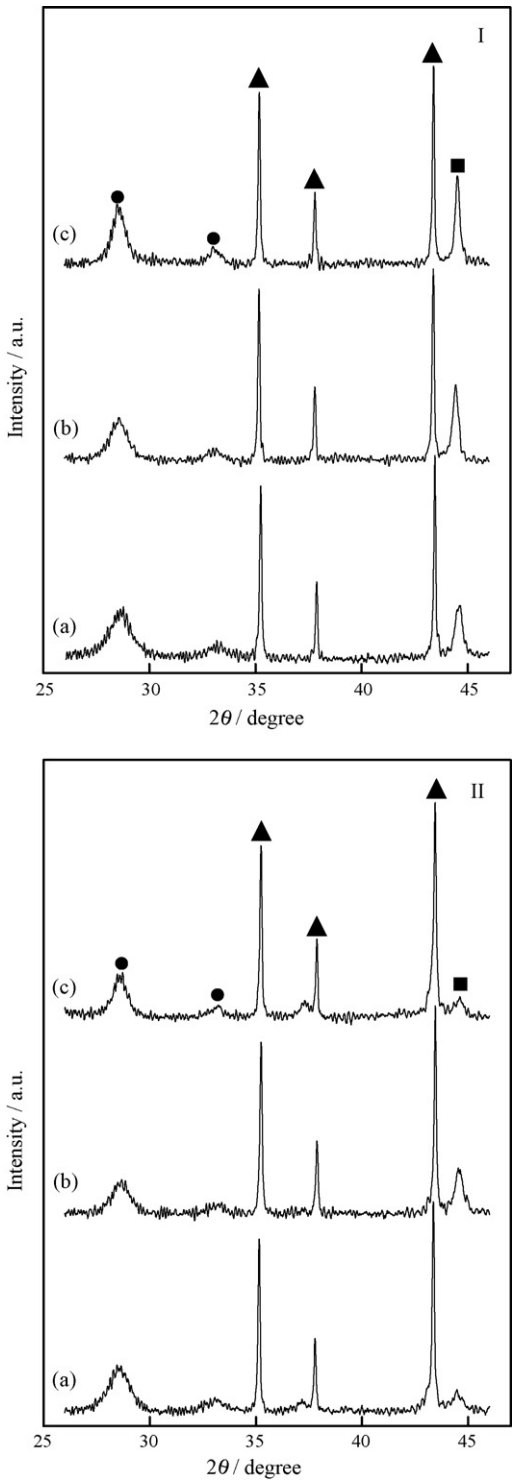


**Fig. 8.** XRD patterns of Pt/Ni/CA (I) and Pt/Ni/CMA (II). (■) Ni; (●) $CeO_2$; (▲) $Al_2O_3$. (a) After $H_2$ reduction, (b) after the reaction at 923 K (Fig. 6) and (c) after the regeneration.

regeneration was determined to be 25.1 nm and 30.5 nm, respectively. This behavior means the aggregation of Ni metal particles. This suggests that the aggregation causes the catalyst deactivation. On the other hand, the average particle size of Ni on Pt/Ni/CMA after the reduction was estimated to be 14.3 nm, which is much larger than that obtained from the TPR and $H_2$ adsorption. This contradiction is associated with the very small intensity of the

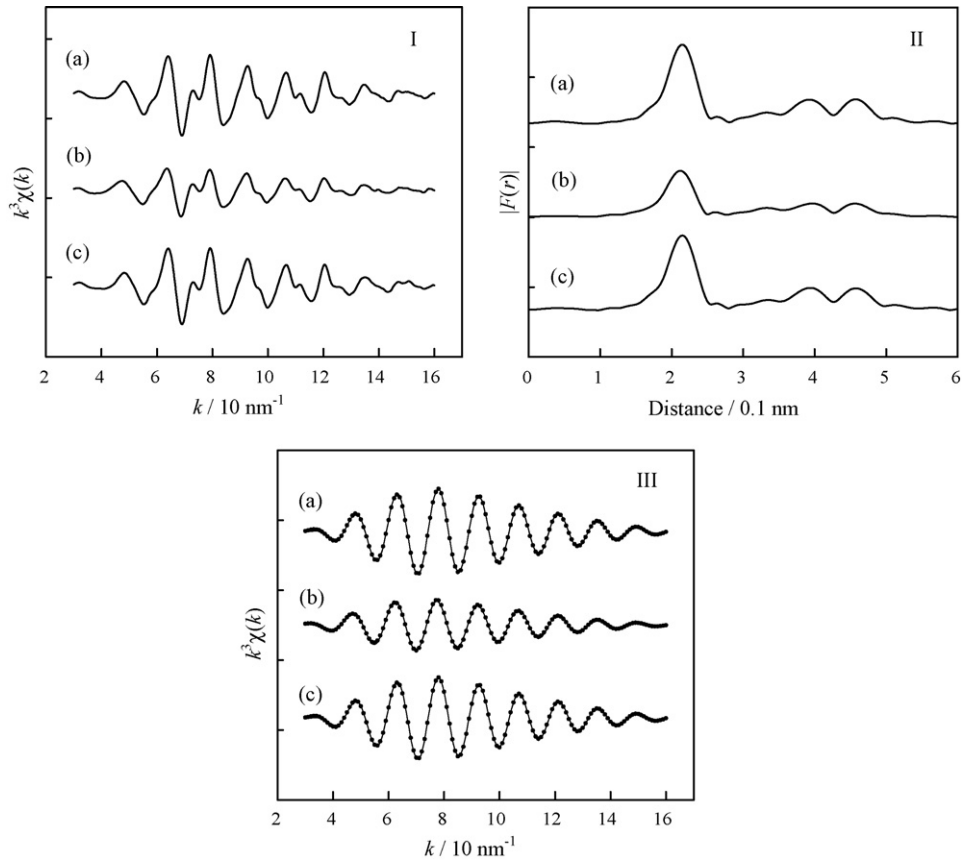


**Fig. 9.** Results of Ni *K*-edge EXAFS analysis of Pt/Ni/CA. (a) After $H_2$ reduction, (b) after the reaction at 923 K (Fig. 6) and (c) after the regeneration. (I) $k^3$-weighted EXAFS oscillation. (II) Fourier transform of $k^3$-weighted Ni *K*-edge EXAFS. FT range: 30–160 nm$^{-1}$. (III) Fourier filtered EXAFS data (solid line) and calculated data (dotted line). Fourier filtering range: 0.126–0.292 nm.

peak due to the Ni metal. The XRD detected large metal particles preferentially, which are not a main component on the Pt/Ni/CMA. In contrast, the adsorption measurement detected small metal particles, which are the main component. The peak intensity due to Ni metal on the Pt/Ni/CMA was increased by the reaction test. This represents the aggregation of Ni metal particles. As shown in Fig. 6, this catalyst showed high catalytic activity at 240 min. Based on this XRD results, it is expected that even Pt/Ni/CMA can be deactivated after a longer activity test. However, an important point is that the Pt/Ni/CMA after the regeneration procedure gave smaller Ni metal peak like that on the catalyst after the reduction. This behavior is greatly different from that on Pt/Ni/CA, where the regeneration procedure also aggregated Ni metal particles. The comparison suggests that the MgO addition can regenerate highly dispersed Ni particles as well as suppress the aggregation of Ni particles.

Fig. 9 shows the Ni *K*-edge EXAFS results of Pt/Ni/CA after $H_2$ reduction, the reaction and regeneration, and the curve fitting results are listed in Table 2. The catalyst after the reaction corresponds to that after the activity test in Fig. 6. The catalyst after the regeneration was prepared by the regeneration of the catalyst after the activity test. The EXAFS spectra of Pt/Ni/CA after all the treatments can be fitted by the single Ni–Ni bond. The coordination number (CN) of the Ni–Ni bond on the catalyst after the reduction was rather large and it increased on the catalyst after the regeneration. This behavior agreed with the XRD results (Fig. 8I). On the other hand, the CN on the catalyst after the reaction was much smaller than that on the catalyst after the reduction and regeneration. This tendency does not agree with the XRD results. According to the previous report, the formation of the nickel carbide during the methane decomposition can weaken the EXAFS oscillation of the Ni metal [46]. In this case, the coke is deposited on the catalysts after the reaction and the nickel carbide may be formed, and this can be a reason for the disagreement of the EXAFS with the XRD results. Further investigation is necessary for the elucidation of the disagreement.

Fig. 10 shows the Ni *K*-edge EXAFS results of the Pt/Ni/CMA and the curve fitting results are also listed in Table 2. The EXAFS spectra of the Pt/Ni/CMA after all the treatments can be fitted with the Ni–O, Ni–Ni, Ni–O–Ni and Ni–O–Mg bonds. The CN of the Ni–Ni bond increased after the reaction and it decreased after the regeneration. The CN of the Ni–Ni bond on the catalyst after the regeneration is almost the same as that after the reduction. The change of CN of the Ni–O bond by treatments is opposite to that of the Ni–Ni bond. The behavior of the CN agreed with the XRD results and the increase of the CN of the Ni–Ni bond by the reaction corresponds to the aggregation, and the CN decrease by the regeneration corresponds to the re-dispersion of Ni metal particles. Another important point is that the Ni–O–Ni and Ni–O–Mg bonds are observed. The CN of the Ni–O–Ni bond is higher than that of the Ni–O–Mg bond. This suggests the formation of the NiO–MgO solid solution with high concentration of NiO. The CN of the Ni–O–Ni bond also decreased by the reaction and increased by the regeneration. This tendency suggests that the re-dispersion proceeds via the formation of the NiO–MgO solid solution and its reduction. In particular, the Ni metal particles formed from the reduction of the NiO–MgO solid solution is expected to be interacted with MgO and $CeO_2$, and to be highly dispersed. They have high resistance to the aggregation during the reaction. This can be supported by previous reports on the effectiveness of NiO–MgO solid solution in methane

**Table 2**
Curve fitting results of Ni *K*-edge EXAFS of the Pt/Ni/CA and Pt/Ni/CMA catalysts

| Catalyst | Condition | Shells | CN[a] | $R$ ($\times 10^{-1}$ nm)[b] | $\sigma$ ($\times 10^{-1}$ nm)[c] | $\Delta E_0$ (eV)[d] | $R_f$ (%)[e] |
|---|---|---|---|---|---|---|---|
| Pt/Ni/CA | Reduction | Ni–Ni | 10.4 ± 1.5 | 2.49 ± 0.008 | 0.073 ± 0.012 | −0.5 ± 2.0 | 0.1 |
| | Reaction | Ni–Ni | 6.8 ± 1.0 | 2.49 ± 0.009 | 0.076 ± 0.012 | −5.0 ± 2.0 | 0.6 |
| | Regeneration | Ni–Ni | 10.7 ± 1.6 | 2.49 ± 0.008 | 0.072 ± 0.012 | −0.7 ± 2.0 | 0.1 |
| Pt/Ni/CMA | Reduction | Ni–O | 2.1 ± 0.2 | 2.10 ± 0.007 | 0.060 ± 0.009 | −2.4 ± 0.5 | 0.9 |
| | | Ni–Ni | 8.5 ± 0.1 | 2.49 ± 0.003 | 0.077 ± 0.001 | −1.1 ± 0.1 | |
| | | Ni–O–Ni | 2.8 ± 0.3 | 2.93 ± 0.005 | 0.068 ± 0.013 | 8.5 ± 0.5 | |
| | | Ni–O–Mg | 1.4 ± 0.4 | 2.94 ± 0.018 | 0.069 ± 0.017 | 3.4 ± 1.4 | |
| | Reaction | Ni–O | 1.8 ± 0.2 | 2.10 ± 0.009 | 0.072 ± 0.018 | −4.7 ± 1.9 | 0.5 |
| | | Ni–Ni | 9.1 ± 0.1 | 2.49 ± 0.001 | 0.069 ± 0.001 | −1.1 ± 0.1 | |
| | | Ni–O–Ni | 2.3 ± 0.1 | 2.93 ± 0.004 | 0.071 ± 0.005 | 8.0 ± 0.6 | |
| | | Ni–O–Mg | 1.3 ± 0.2 | 2.94 ± 0.000 | 0.071 ± 0.019 | −5.3 ± 1.7 | |
| | Regeneration | Ni–O | 2.1 ± 0.8 | 2.10 ± 0.018 | 0.068 ± 0.013 | −3.3 ± 1.7 | 0.9 |
| | | Ni–Ni | 8.6 ± 0.1 | 2.49 ± 0.000 | 0.077 ± 0.001 | −0.9 ± 0.2 | |
| | | Ni–O–Ni | 2.7 ± 0.1 | 2.93 ± 0.006 | 0.063 ± 0.004 | 6.7 ± 0.6 | |
| | | Ni–O–Mg | 1.4 ± 0.5 | 2.94 ± 0.017 | 0.061 ± 0.020 | 5.1 ± 1.6 | |
| Ni foil | – | Ni–Ni | 12 | 2.49 | 0.060 | 0.0 | – |
| NiO | – | Ni–O | 6 | 2.10 | 0.060 | 0.0 | – |
| | – | Ni–O–Ni | 12 | 2.94 | 0.060 | 0.0 | |

Fourier transform range: 30–160 nm$^{-1}$; Fourier filtering range: 0.126–0.292 nm.
[a] Coordination number.
[b] Bond distance.
[c] Debye–Waller factor.
[d] Difference in the origin of photoelectron energy between the reference and the sample.
[e] Residual factor.

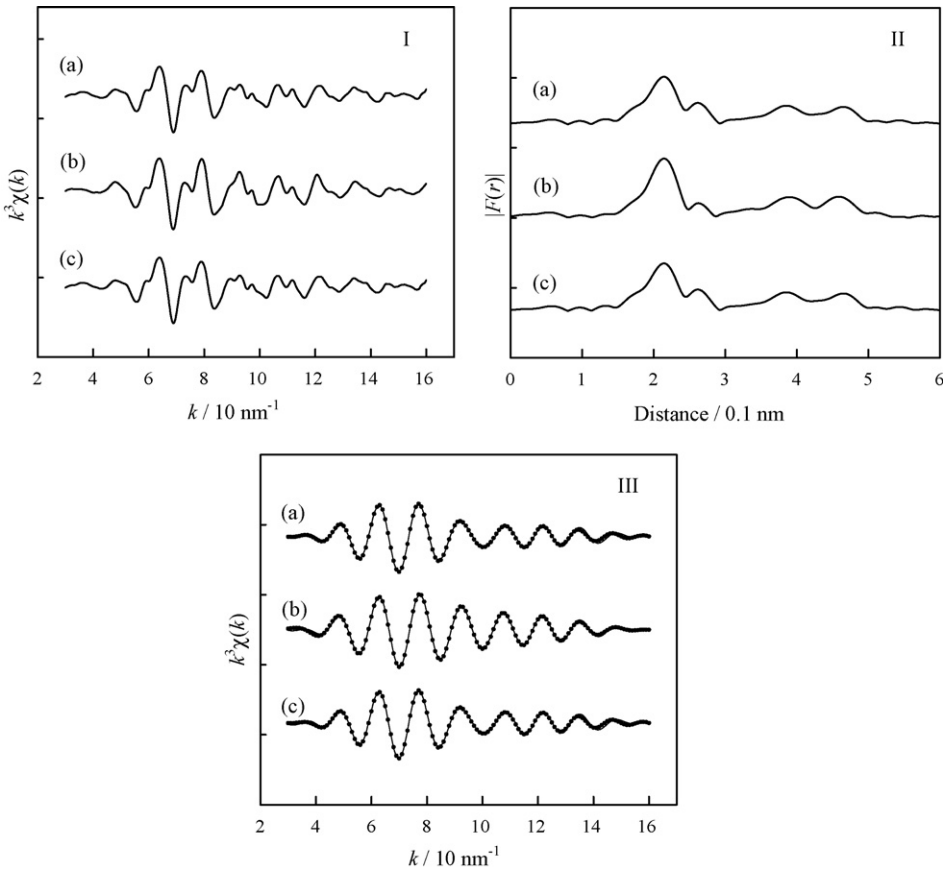


**Fig. 10.** Results of Ni *K*-edge EXAFS analysis of Pt/Ni/CMA. (a) After $H_2$ reduction, (b) after the reaction at 923 K (Fig. 6) and (c) after the regeneration. (I) $k^3$-weighted EXAFS oscillation. (II) Fourier transform of $k^3$-weighted Ni *K*-edge EXAFS. FT range: 30–160 nm$^{-1}$. (III) Fourier filtered EXAFS data (solid line) and calculated data (dotted line). Fourier filtering range: 0.126–0.292 nm.

conversion to synthesis gas by steam reforming, $CO_2$ reforming, and oxidative reforming [31,32,38–40,42,47,48].

## 4. Conclusions

1. The catalytic performance of the $Pt/Ni/CeO_2/MgO/Al_2O_3$ was as high as that of the $Pt/Ni/CeO_2/Al_2O_3$ in steam gasification of cedar wood.
2. The $Pt/Ni/CeO_2/MgO/Al_2O_3$ was activated automatically by the reactants in the steam gasification. The activation rate was not so high as that of the $Pt/Ni/CeO_2/Al_2O_3$.
3. The addition of MgO to $Pt/Ni/CeO_2/Al_2O_3$ decreased the Ni reducibility and promoted the dispersion of Ni metal particles via the formation of NiO–MgO solid solution.
4. The $Pt/Ni/CeO_2/Al_2O_3$ was deactivated during the steam gasification and this deactivation can be caused by the aggregation of the Ni metal particles.
5. The catalyst stability of the $Pt/Ni/CeO_2/MgO/Al_2O_3$ was much higher than that of the $Pt/Ni/CeO_2/Al_2O_3$. The aggregation of the Ni metal particles on the $Pt/Ni/CeO_2/MgO/Al_2O_3$ is not so significant as that on the $Pt/Ni/CeO_2/Al_2O_3$. High resistance to the aggregation is given by the addition of MgO.
6. In the case of the $Pt/Ni/CeO_2/MgO/Al_2O_3$, the aggregation of Ni metal particles proceeded to some extent during the reaction, however, the aggregated Ni particles became highly dispersed by the catalyst regeneration (oxidation and reduction). The re-dispersion can proceed via the formation of the NiO–MgO solid solution by oxidation and the reduction of the NiO–MgO.

## Acknowledgements

A part of this research was supported by Fukuoka Strategy Conference for Hydrogen Energy and Nippon Steel Corporation.

## References

[1] G.W. Huber, S. Iborra, A. Corma, Chem. Rev. 106 (2006) 4044.
[2] R.M. Navarro, M.A. Pena, J.L.G. Fierro, Chem. Rev. 107 (2007) 3952.
[3] K. Tomishige, M. Asadullah, K. Kunimori, Catal. Today 89 (2004) 389.
[4] M. Asadullah, K. Tomishige, K. Fujimoto, Catal. Commun. 2 (2001) 63.
[5] M. Asadullah, S. Ito, K. Kunimori, M. Yamada, K. Tomishige, J. Catal. 208 (2002) 255.
[6] M. Asadullah, S. Ito, K. Kunimori, M. Yamada, K. Tomishige, Environ. Sci. Technol. 36 (2002) 4476.
[7] M. Asadullah, T. Miyazawa, S. Ito, K. Kunimori, K. Tomishige, Appl. Catal. A: Gen. 246 (2003) 103.
[8] M. Asadullah, T. Miyazawa, S. Ito, K. Kunimori, M. Yamada, K. Tomishige, Appl. Catal. A: Gen. 255 (2003) 169.
[9] K. Tomishige, T. Miyazawa, M. Asadullah, S. Ito, K. Kunimori, Green Chem. 5 (2003) 399.
[10] M. Asadullah, T. Miyazawa, S. Ito, K. Kunimori, S. Koyama, K. Tomishige, Biomass Bioenergy 26 (2004) 269.
[11] M. Asadullah, T. Miyazawa, S. Ito, K. Kunimori, M. Yamada, K. Tomishige, Appl. Catal. A: Gen. 267 (2004) 95.
[12] T. Miyazawa, T. Abe, K. Kunimori, K. Tomishige, J. Jpn. Petrol. Inst. 48 (2005) 162.
[13] K. Tomishige, T. Miyazawa, T. Kimura, K. Kunimori, Catal. Commun. 6 (2005) 37.
[14] K. Tomishige, T. Miyazawa, T. Kimura, K. Kunimori, N. Koizumi, M. Yamada, Appl. Catal. B: Environ. 60 (2005) 299.
[15] T. Miyazawa, T. Kimura, J. Nishikawa, K. Kunimori, K. Tomishige, Sci. Technol. Adv. Mater. 6 (2005) 604.
[16] P.J. Dauenhauer, B.J. Dreyer, N.J. Degenstein, L.D. Schmidt, Angew. Chem. Int. Ed. 46 (2007) 5864.
[17] D. Wang, S. Czernik, E. Chornet, Energy Fuels 12 (1998) 19.
[18] D. Wang, S. Czernik, D. Montane, M. Mann, E. Chornet, Ind. Eng. Chem. Res. 36 (1997) 1507.
[19] M. Asadullah, T. Miyazawa, S. Ito, K. Kunimori, K. Tomishige, Energy Fuels 17 (2003) 842.
[20] K. Tomishige, T. Miyazawa, M. Asadullah, S. Ito, K. Kunimori, J. Jpn. Petrol. Inst. 46 (2003) 322.
[21] T. Miyazawa, T. Kimura, J. Nishikawa, S. Kado, K. Kunimori, K. Tomishige, Catal. Today 115 (2006) 254.
[22] K. Tomishige, T. Kimura, J. Nishikawa, T. Miyazawa, K. Kunimori, Catal. Commun. 8 (2007) 1074.
[23] T. Kimura, T. Miyazawa, J. Nishikawa, T. Miyao, S. Naito, K. Okumura, K. Kunimori, K. Tomishige, Appl. Catal. B: Environ. 68 (2006) 160.
[24] J. Nishikawa, T. Miyazawa, K. Nakamura, M. Asadullah, K. Kunimori, K. Tomishige, Catal. Commun. 9 (2008) 195.
[25] J. Nishikawa, K. Nakamura, M. Asadullah, T. Miyazawa, K. Kunimori, K. Tomishige, Catal. Today 131 (2008) 146.
[26] K. Sato, K. Fujimoto, Catal. Commun. 8 (2007) 1697.
[27] T. Furusawa, A. Tsutsumi, Appl. Catal. A: Gen. 278 (2005) 207.
[28] T. Furusawa, A. Tsutsumi, Appl. Catal. A: Gen. 278 (2005) 195.
[29] K. Tasaka, T. Furusawa, A. Tsutsumi, Energy Fuels 21 (2007) 590.
[30] K. Tomishige, Y. Himeno, Y. Matsuo, Y. Yoshinaga, Y. Fujimoto, Ind. Eng. Chem. Res. 39 (2000) 1891.
[31] K. Tomishige, Y.G. Chen, K. Fujimoto, J. Catal. 181 (1999) 91.
[32] O. Yamazaki, K. Tomishige, K. Fujimoto, Appl. Catal. A: Gen. 136 (1996) 49.
[33] C.H. Bartholomew, Catal. Rev. Sci. Eng. 24 (1982) 67.
[34] J.W. Cook, D.E. Sayers, J. Appl. Phys. 52 (1981) 5024.
[35] K. Okumura, J. Amano, N. Yasunobu, M. Niwa, J. Phys. Chem. B 104 (2000) 1050.
[36] K. Okumura, S. Matsumoto, N. Nishiaki, M. Niwa, Appl. Catal. B: Environ. 40 (2003) 151.
[37] A.L. Ankudinov, B. Ravel, J.J. Rehr, S.D. Conradson, Phys. Rev. B 58 (1998) 7565.
[38] M. Nurunnabi, B.T. Li, K. Kunimori, K. Suzuki, K. Fujimoto, K. Tomishige, Appl. Catal. A: Gen. 292 (2005) 272.
[39] M. Nurunnabi, B.T. Li, K. Kunimori, K. Suzuki, K. Fujimoto, K. Tomishige, Catal. Lett. 103 (2005) 277.
[40] M. Nurunnabi, Y. Mukainakano, S. Kado, B.T. Li, K. Kunimori, K. Suzuki, K. Fujimoto, K. Tomishige, Appl. Catal. A: Gen. 299 (2006) 145.
[41] B.T. Li, R. Watanabe, K. Maruyama, M. Nurunnabi, K. Kunimori, K. Tomishige, Appl. Catal. A: Gen. 290 (2005) 36.
[42] Y. Chen, K. Tomishige, K. Yokoyama, K. Fujimoto, J. Catal. 184 (1999) 479.
[43] K. Tomishige, A. Okabe, K. Fujimoto, Appl. Catal. A: Gen. 194 (2000) 383.
[44] R. Ueda, T. Kusakari, K. Tomishige, K. Fujimoto, J. Catal. 194 (2000) 14.
[45] Z. Hu, T. Wakasugi, A. Maeda, K. Kunimori, T. Uchijima, J. Catal. 127 (1991) 276.
[46] S. Takenaka, Y. Shigeta, E. Tanabe, K. Otsuka, J. Phys. Chem. B 108 (2004) 7656.
[47] Y.H. Hu, E. Ruckenstein, Adv. Catal. 48 (2004) 297.
[48] Y.H. Hu, E. Ruckenstein, Catal. Rev. Sci. Eng. 44 (2002) 423.